Electronic Supplementary Material (ESI) for Journal of Materials Chemistry A.
This journal is © The Royal Society of Chemistry 2021

Supporting Information

Argentophilic pyridinic nitrogen for embedding lithiophilic silver nanoparticles in three-dimensional carbon scaffold for reversible lithium plating/stripping

Yuju Jeon,[‡,a,c] Jonghak Kim,[‡,a] Haeseong Jang,[b] Jeongin Lee,[a] Min Gyu Kim,[b] Nian Liu[*,c] and Hyun-Kon Song[*,a]

[a] School of Energy and Chemical Engineering, UNIST, Ulsan 44919, Korea

[b] Beamline Research Division, Pohang Accelerator Laboratory (PAL), Pohang 790-784, Korea

[c] School of Chemical & Biomolecular Engineering, Georgia Institute of Technology, Atlanta, Georgia 30332, United States

[*] Correspondence should be addressed to N.L. (email: nian.liu@chbe.gatech.edu) and H.-K.S. (email: philiphobi@hotmail.com).

[‡] These authors contributed equally to this work.

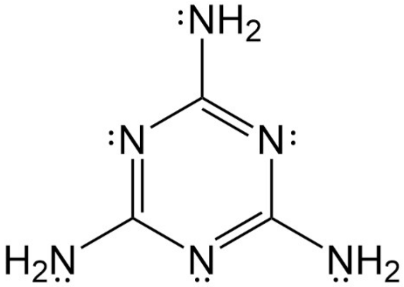

Fig. S1 Molecular structure of melamine.

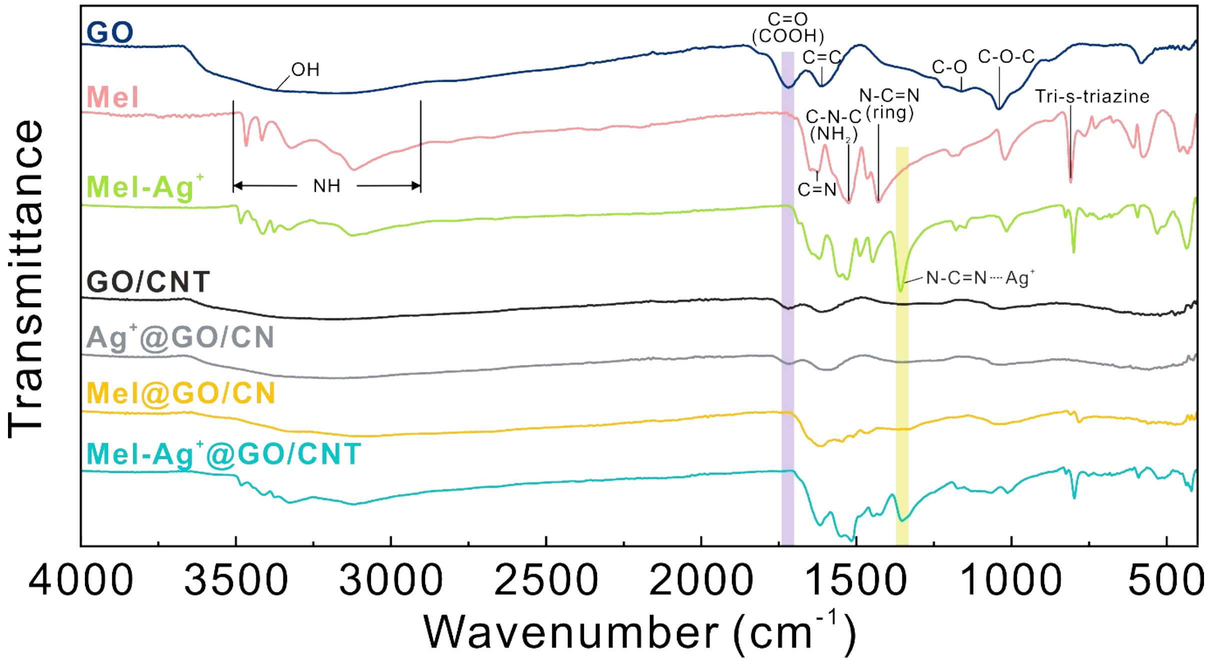

Fig. S2 Infrared spectra.

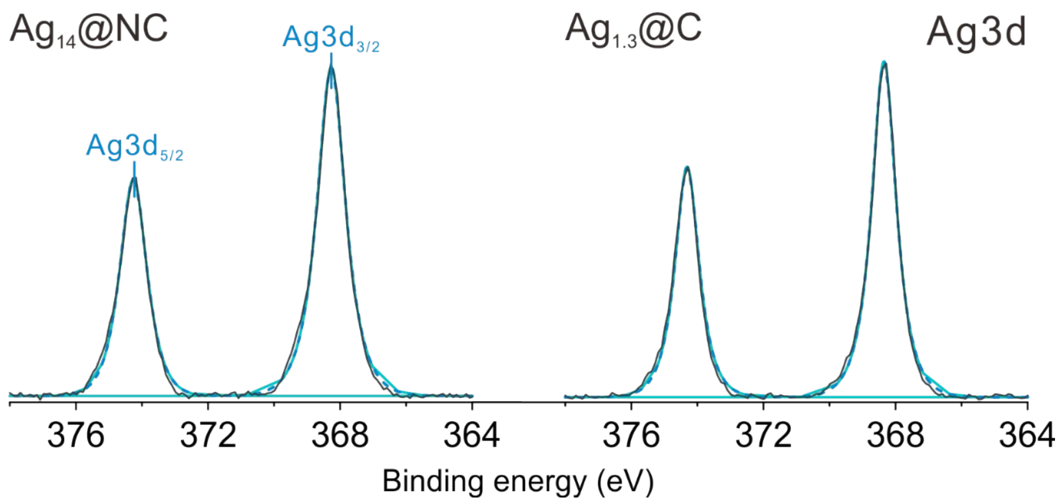

Fig. S3 XPS Ag 3d spectra of Ag$_{14}$@NC and Ag$_{1.3}$@C.

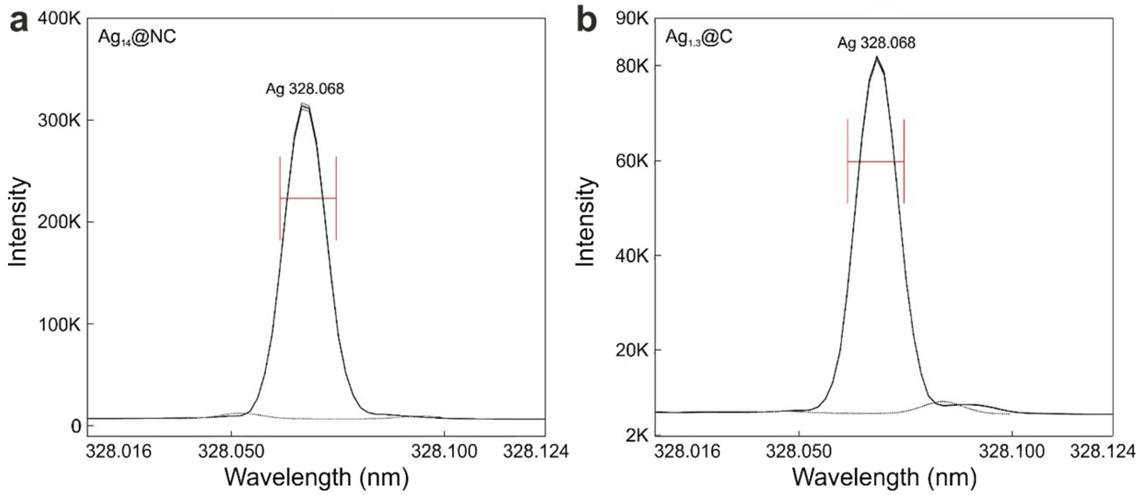

Fig. S4 Inductively coupled plasma-optical emission spectrometric (ICP-OES) silver spectra. (a) Ag$_{14}$@NC. (b) Ag$_{1.3}$@C. The silver intensity of Ag$_{14}$@NC was four times higher than that of Ag$_{1.3}$@C, which is consistent with the weight difference in silver loading amount between Ag$_{14}$@NC and Ag$_{1.3}$@C scaffolds.

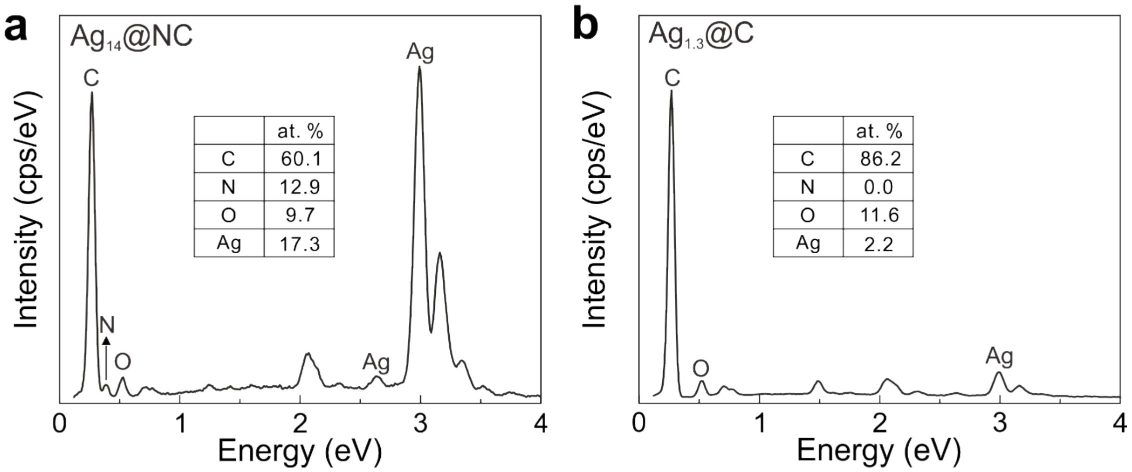

	at. %
C	60.1
N	12.9
O	9.7
Ag	17.3

	at. %
C	86.2
N	0.0
O	11.6
Ag	2.2

Fig. S5 EDS quantification for silver. (a) Ag_{14}@NC. (b) $Ag_{1.3}$@C.

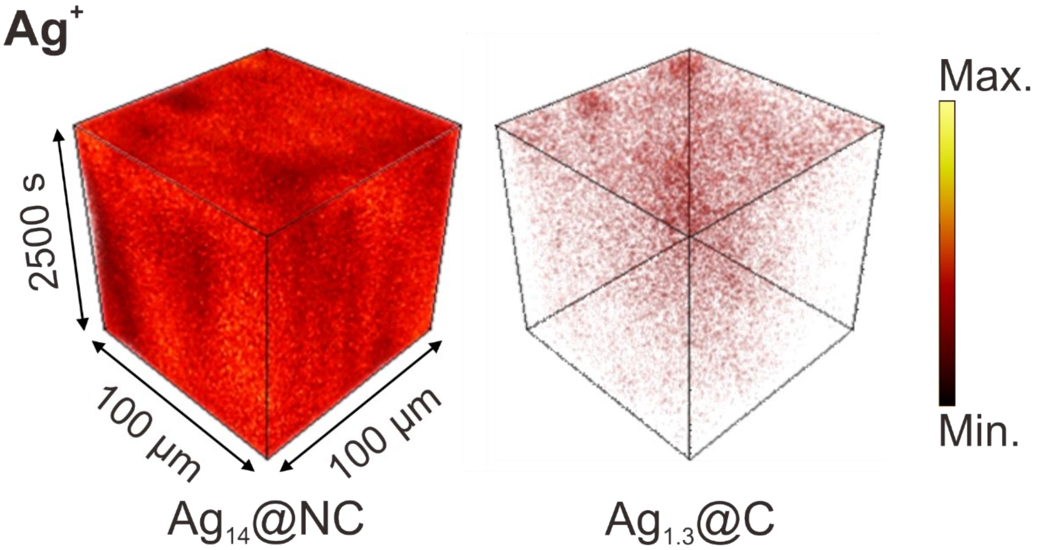

Fig. S6 Three-dimensional time-of-flight secondary ion mass spectroscopy (TOF-SIMS) images of Ag_{14}@NC and $Ag_{1.3}$@C on Ag^+ obtained during depth profiling of Fig. 3b.

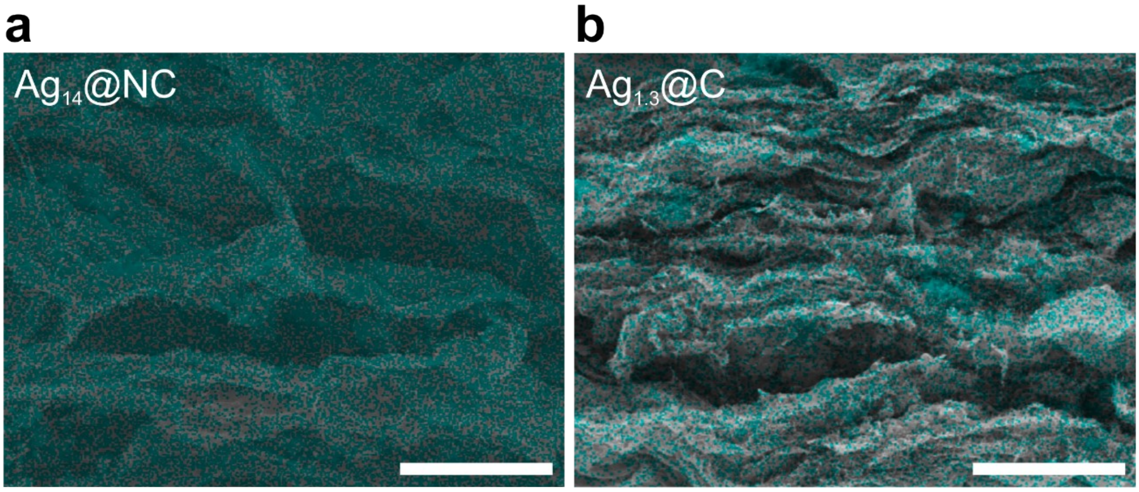

Fig. S7 Silver-mapped cross-sectional scanning-electron-microscopic (SEM) images. (a) Ag_{14}@NC. (b) $Ag_{1.3}$@C. Silver atoms were identified as turquoise color. Scale bar: 10 μm.

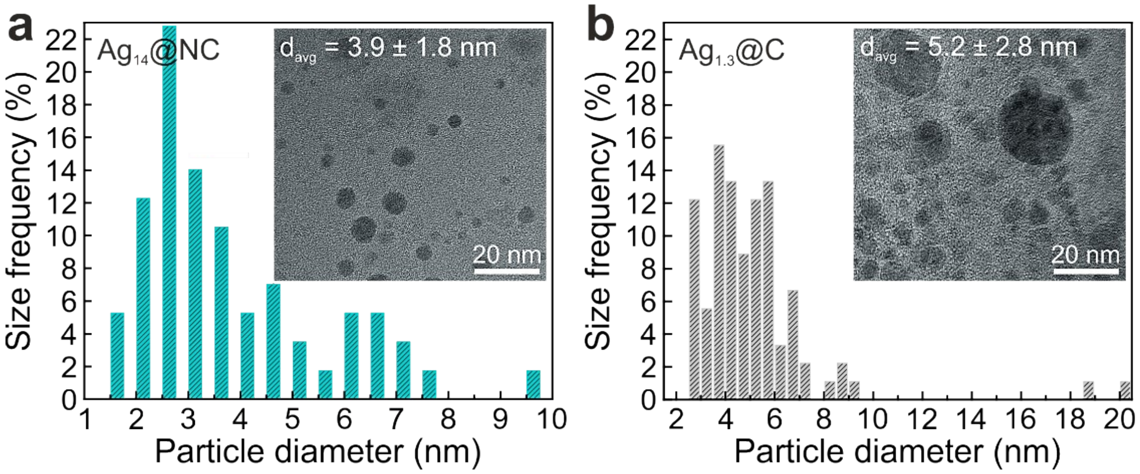

Fig. S8 Size distribution of silver nanoparticles. (a) Ag_{14}@NC. (b) $Ag_{1.3}$@C. The insets in (a) and (b) are the transmission-electron-microscopic (TEM) images of silver nanoparticles on the matrix of Ag_{14}@NC and $Ag_{1.3}$@C.

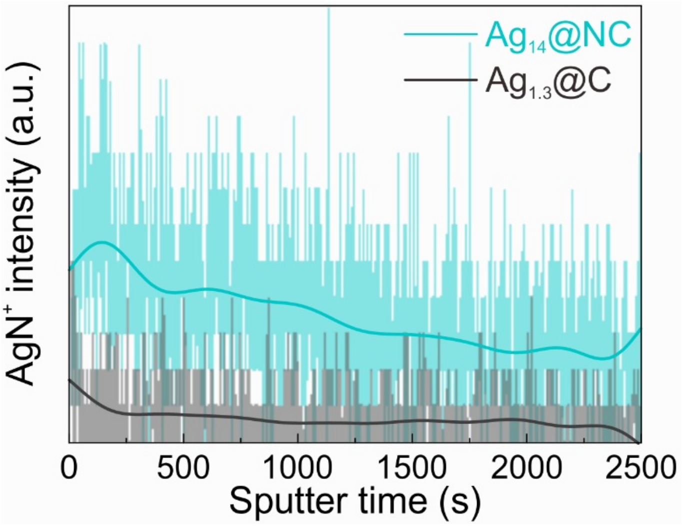

Fig. S9 TOF-SIMS depth profiling spectra of Ag_{14}@NC and $Ag_{1.3}$@C on AgN^+ over 2500 s of O_2^+ sputtering.

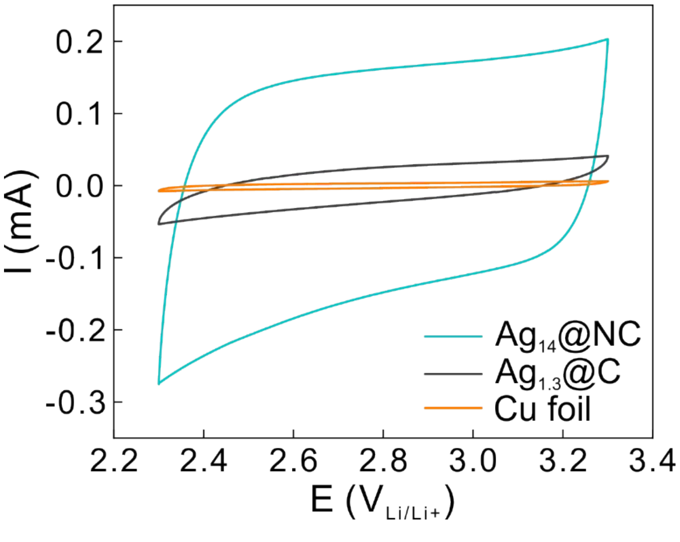

Fig. S10 Cyclic voltammetry of Ag_{14}@NC, $Ag_{1.3}$@C and Cu foil in capacitive voltage region. The capacitance of Ag_{14}@NC, $Ag_{1.3}$@C and Cu foil was 20, 3 and 0.4 mF cm^{-2}, respectively. The apparent area of Ag_{14}@NC, $Ag_{1.3}$@C and Cu foil was equal to 0.785 cm^2.

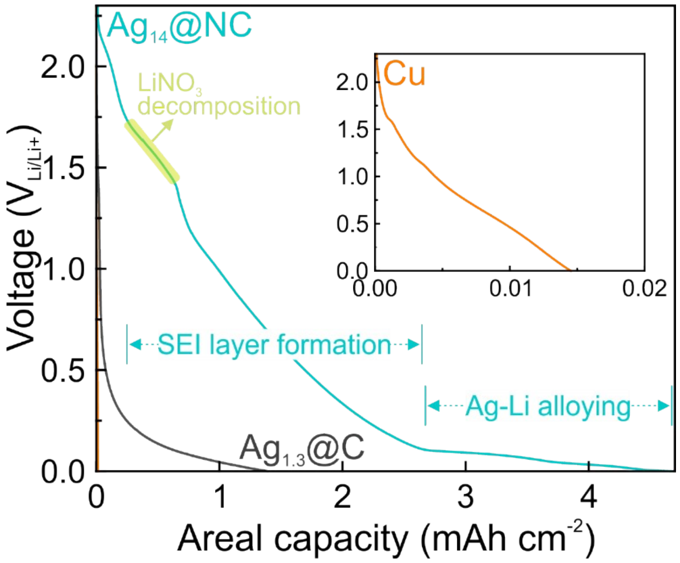

Fig. S11 Reduction voltage profiles of Ag$_{14}$@NC, Ag$_{1.3}$@C and Cu above 0 V$_{Li/Li+}$ in galvanostatic mode at 0.05 mA cm^{-2}.

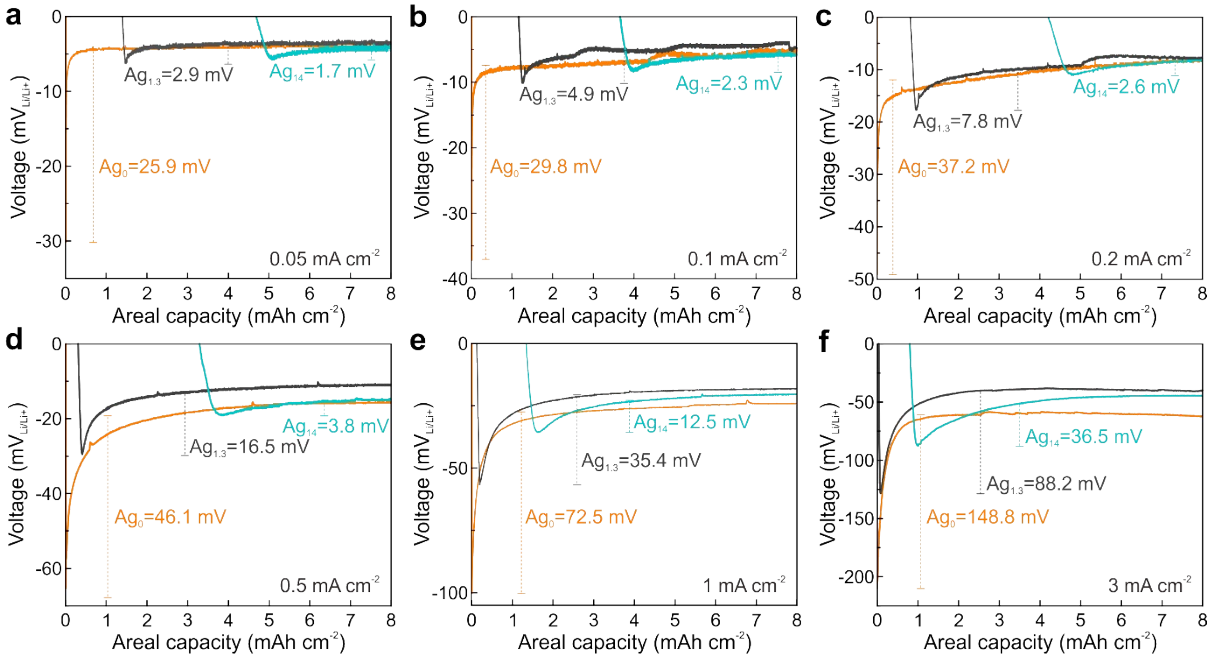

Fig. S12 Voltage profiles of lithium metal plating at various current densities in Ag$_{14}$@NC||Li, Ag$_{1.3}$@C||Li and Cu||Li cells. (a) 0.05 mA cm^{-2}. (b) 0.1 mA cm^{-2}. (c) 0.2 mA cm^{-2}. (d) 0.5 mA cm^{-2}. (e) 1 mA cm^{-2}. (f) 3 mA cm^{-2}.

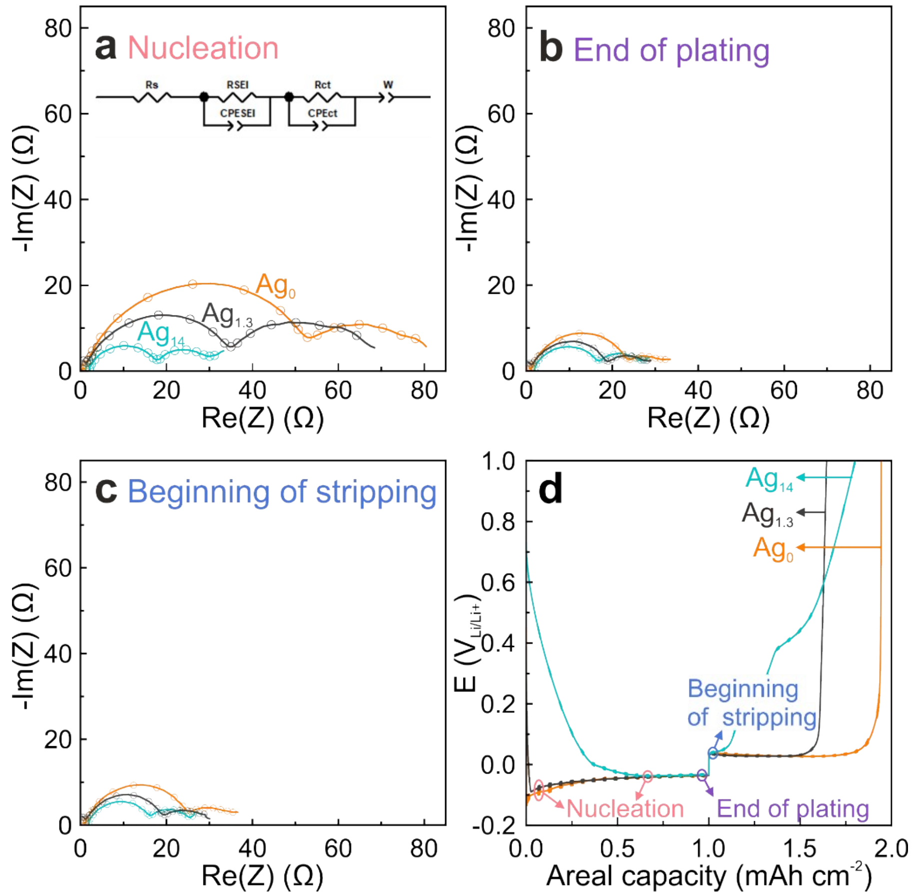

Fig. S13 *in situ* galvanostatic electrochemical impedance spectroscopy (GEIS) measurement of Ag_{14}@NC||Li, $Ag_{1.3}$@C||Li and Cu||Li during lithium plating and stripping at 1 mA cm^{-2}. (a) Nucleation. The inset is equivalent circuit used for fitting in situ GEIS spectra in Fig. S11a-c. (b) End of plating. (c) Beginning of stripping. (d) Voltage profiles of lithium plating and stripping at 1 mA cm^{-2} during *in situ* GEIS measurement. Lithium was plated up to 1 mAh cm^{-2}. The points at which in situ GEIS was conducted are shown as potential pulses. Lithium plating and stripping was monitored *in situ* by galvanostatic electrochemical impedance spectroscopy (GEIS). The constant current at 1 mA cm^{-2} coupled with a small-amplitude sinusoidal current function was applied to lithium metal cells of the 3D scaffold electrodes for lithium metal plating on the 3D scaffolds followed by stripping.[1] Impedance spectra (Fig. S13a-c) were obtained along voltage profiles of plating and stripping (Fig. S13d). Two semicircles were obtained for all samples (the equivalent circuit in the inset of Fig. S13a). The highfrequency semicircle was relevant to the de-solvation process of solvated lithium ions when the ions moved from electrolyte to the SEI layer (R_{SEI}). The low-frequency semicircle was assigned to the charge transfer process of transformation of lithium ion to lithium metal (R_{ct}).

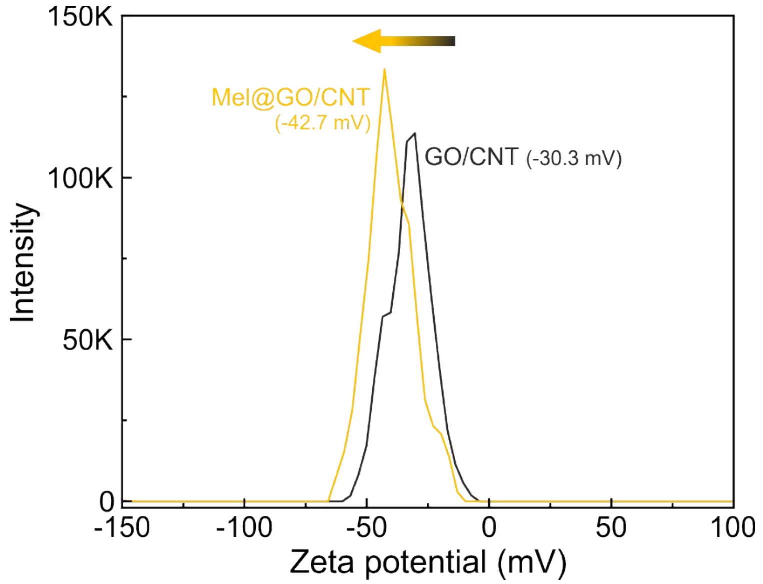

Fig. S14 Zeta potential measurement on GO/CNT and Mel@GO/CNT solutions.

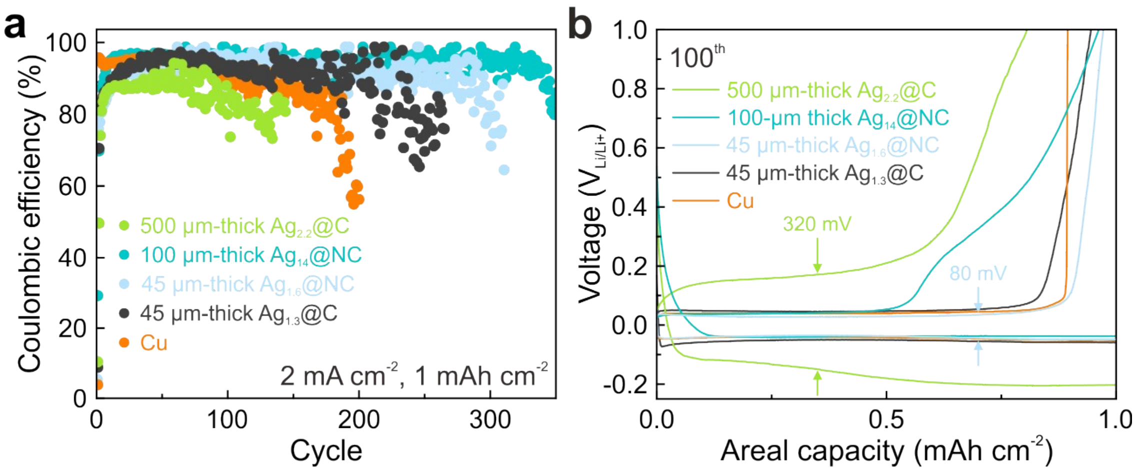

Fig. S15 (a) Coulombic efficiency of 500 μm-thick $Ag_{2.2}$@C||Li, 100 μm-thick Ag_{14}@NC||Li, 45 μm-thick $Ag_{1.6}$@NC||Li, 45 μm-thick $Ag_{1.3}$@C||Li and Cu||Li cells for repeated lithium plating and stripping cycles at 2 mA cm^{-2}. Lithium metal was plated up to 1 mAh cm^{-2}. (b) Voltage profiles of 100th cycle.

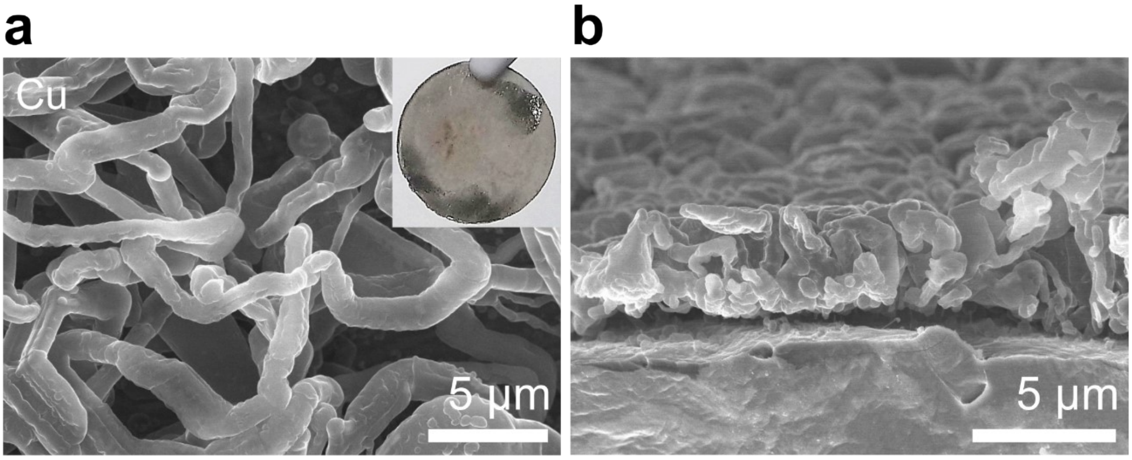

Fig. S16 Lithium metal morphology of Cu after lithium plating of 1 mAh cm^{-2} at 1 mA cm^{-2} visualized by SEM. (a) Surface. (b) Cross-section. The inset in (a) is the photo of the lithium metal plated on Cu.

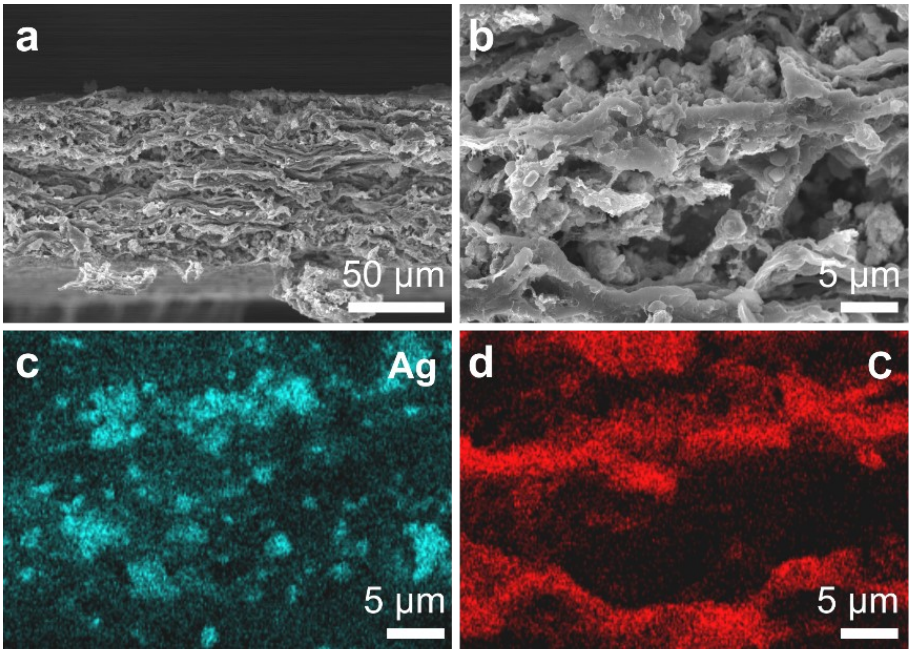

Fig. S17 Lithium-stripped Ag$_{14}$@NC after 50 cycles of lithium plating and stripping at 2 mA cm^{-2}. (a and b) Cross-sectional morphology of Ag$_{14}$@NC by SEM. (a) Low-magnification image. (b) High-magnification image. (c and d) EDS map of (b). The detected elements were indicated. Lithium metal was plated up to 1 mAh cm^{-2} during the cycles.

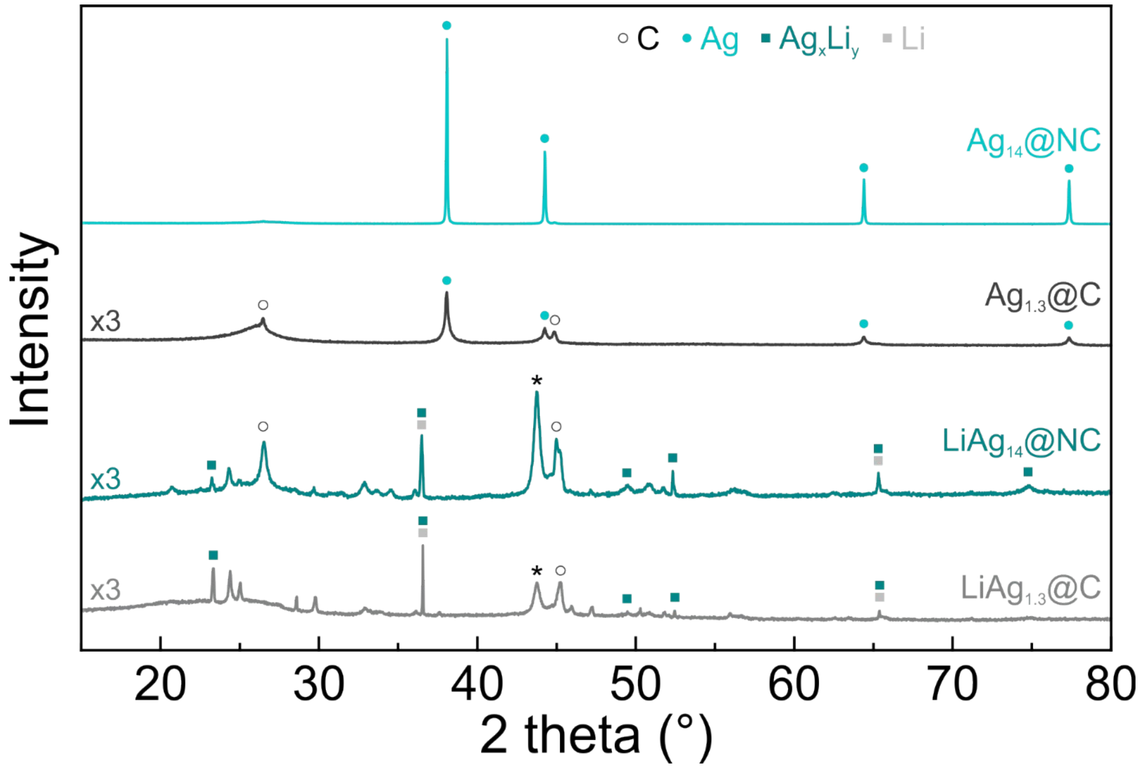

Fig. S18 X-ray diffraction (XRD) pattern of Ag_{14}@NC, $Ag_{1.3}$@C, $LiAg_{14}$@NC and $LiAg_{1.3}$@C. The asterisk (*) at 44° indicates the peak of XRD sample holder.

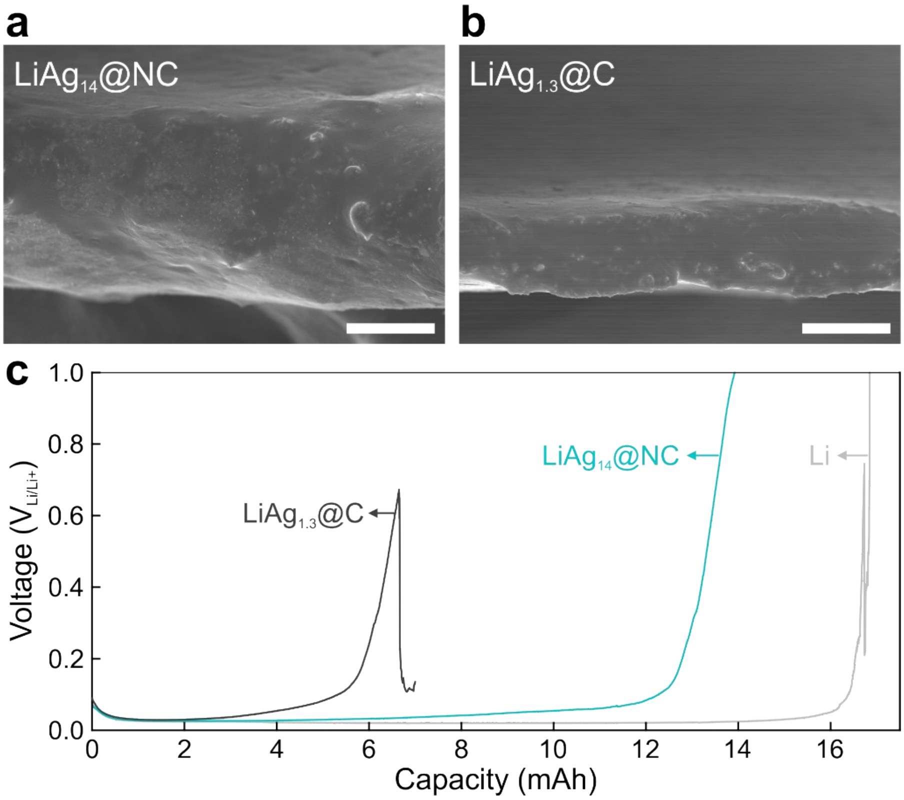

Fig. S19 (a and b) Morphology of lithium infused scaffolds visualized by SEM. (a) $LiAg_{14}$@NC. (b) $LiAg_{1.3}$@C. Scale bar: 50 μm for (a) and (b). (c) Voltage profile of lithium stripping at 1 mA cm^{-2}. The stripping capacity was 6.7, 14 and 16.8 mAh for $LiAg_{1.3}$@C, $LiAg_{14}$@NC and Li, respectively.

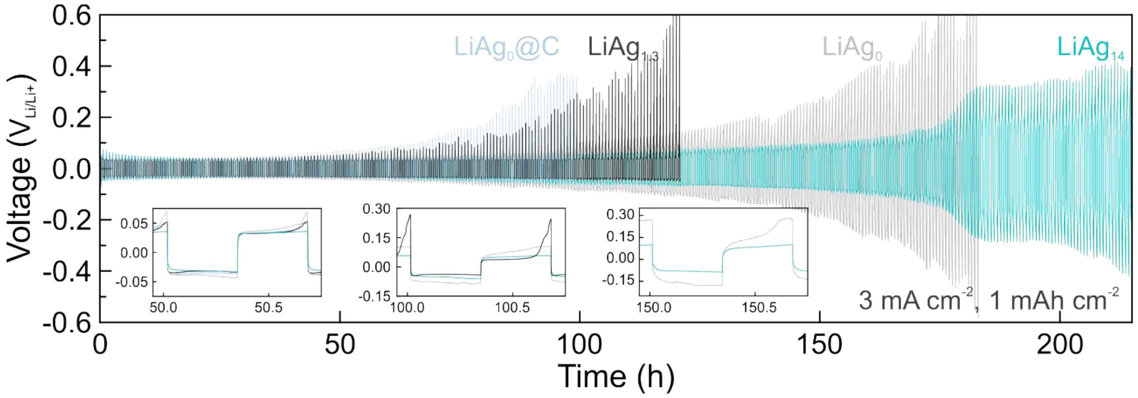

Fig. S20 Voltage profiles of symmetric cells (LiAg$_{14}$@NC||Li, LiAg$_{1.3}$@C||Li, LiAg$_0$@C||Li and Li||Li). Lithium metal was plated and stripped at 3 mA cm^{-2} up to 1 mAh cm^{-2}.

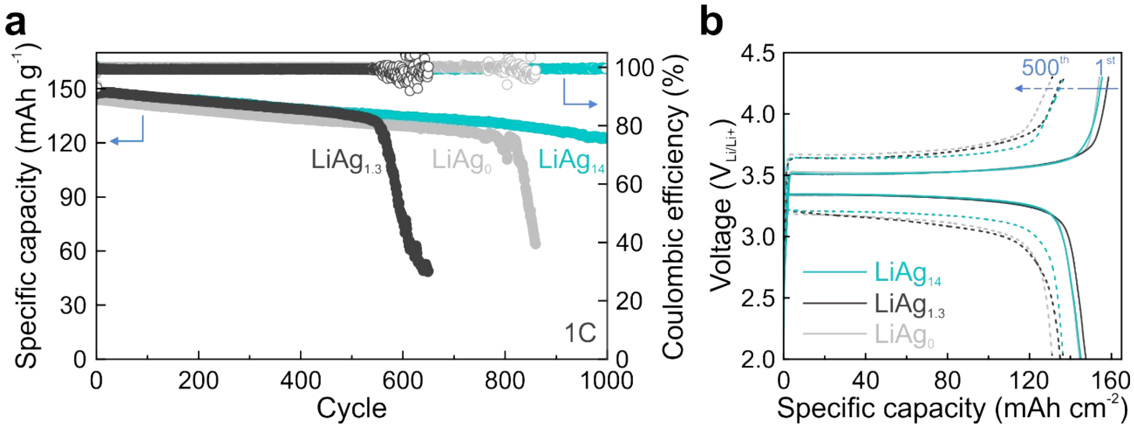

Fig. S21 (a) Retention of capacity and coulombic efficiency of lithium iron phosphate (LFP)-based full cells (LiAg$_{14}$@NC||LFP, LiAg$_{1.3}$@C||LFP and Li||LFP) at 1C (1C = 1 mA cm^{-2}). (b) Voltage profiles of the 1st and 500th cycle in (a).

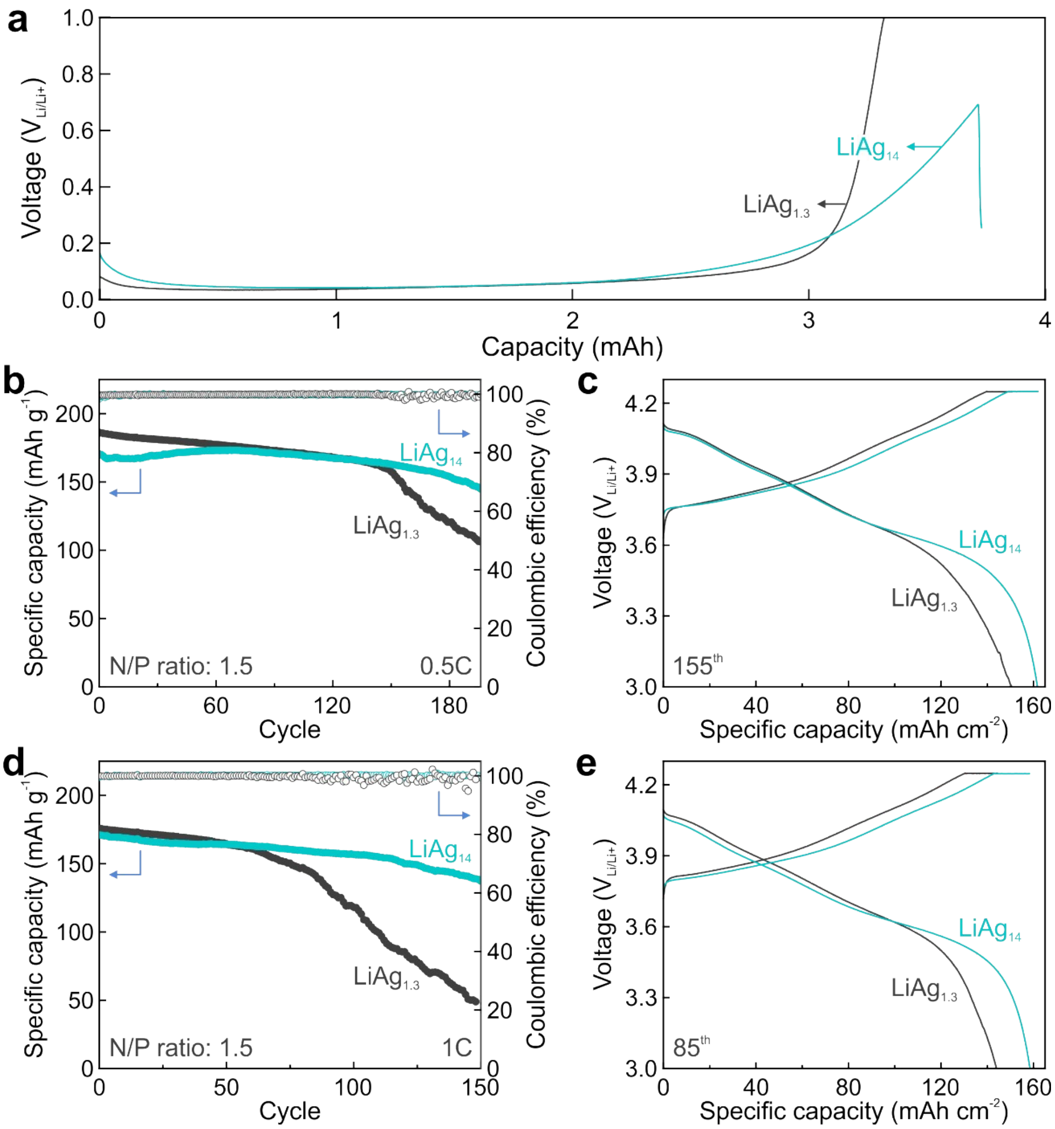

Fig. S22 Practical application of LiAg$_{14}$@NC scaffold with limited lithium amount. (a) Voltage profile of lithium stripping at 1 mA cm^{-2}. The stripping capacity was 3.3 and 3.7 mAh for LiAg$_{1.3}$@C and LiAg$_{14}$@NC, respectively. The reversible capacity for full cell operation was regarded as 3.0 mAh (up to 0.2 V$_{Li/Li+}$) for both scaffolds. (b-e) Lithium metal plating and stripping in LiNi$_{0.8}$Co$_{0.1}$M$_{0.1}$O$_2$-based full cells (LiAg$_{14}$@NC||NCM811 and LiAg$_{1.3}$@C|| NCM811, 1C = 2.5 mA cm^{-2}). (b) Retention of capacity and coulombic efficiency at 0.5C. (c) Voltage profiles of the 155th cycle in (b). (d) Retention of capacity and coulombic efficiency at 1C. (e) Voltage profiles of the 85th cycle in (d).

Table S1 Full-cell performance comparison with previously reported works.

3D scaffold based on GO/rGO/CNT/Ag NP	Cathode	Current density (mA cm^{-2})	Cycling capacity (mAh cm^{-2})	Cycles	Capacity retention (%)	Ref.
LiAg$_{14}$@NC	**LFP**	**2.85**	**0.95**	**805**	**80**	**This work**
	NCM811	**2.5**	**2.5**	**150**	**80**	
	O_2	**0.20**	**0.20**	**183**	**100**	
3D G/Li	LFP	0.85	1.70	80	94	2
CF/Ag-Li	LFP	0.83	0.83	500	63	3
Li/CNT	LFP	1.00	2.50	150	93	4
Li@3D-AGBN	NCM523	2.17	0.22	1000	48	5
N-doped graphene-Li	LFP	0.23	0.45	500	88	6
CNT/PANI@Li	LFP	0.06	0.11	100	68	7
GAL	LFP	0.51	0.51	300	96	8
Li@VGA	LFP	1.25	2.50	400	90	9
	NCM622	2.05	4.10	150	87	
CC/Ag/Li	LFP	0.73	0.73	320	99	10
Li@CNTs/CNFs	LFP	0.85	0.85	150	99	11
PPy/rGO@Li	LFP	0.43	0.43	200	97	12
Li@eGF	LFP	1.62	3.24	200	81	13
Ag@CMFs-Li	LFP	0.68	0.68	250	96	14
GCNT-Li	LFP	1.24	0.31	570	98	15
	NCM811	1.21	0.61	470	83	

References

1. Y. Ko, Y.-G. Cho and H.-K. Song, *RSC Adv.*, 2014, **4**, 16545.
2. W. Deng, X. Zhou, Q. Fang and Z. Liu, *Adv. Energy Mater.*, 2018, **8**, 1703152.
3. R. Zhang, X. Chen, X. Shen, X.-Q. Zhang, X.-R. Chen, X.-B. Cheng, C. Yan, C.-Z. Zhao and Q. Zhang, *Joule*, 2018, **2**, 764-777.
4. Z. Sun, S. Jin, H. Jin, Z. Du, Y. Zhu, A. Cao, H. Ji and L.-J. Wan, *Adv. Mater.*, 2018, **30**, 1800884.
5. P. Xue, S. Liu, X. Shi, C. Sun, C. Lai, Y. Zhou, D. Sui, Y. Chen and J. Liang, *Adv. Mater.*, 2018, **30**, 1804165.
6. G. Huang, J. Han, F. Zhang, Z. Wang, H. Kashani, K. Watanabe and M. Chen, *Adv. Mater.*, 2019, **31**, 1805334.
7. M. Zhang, R. Lu, H. Yuan, K. Amin, L. Mao, W. Yan and Z. Wei, *ACS Appl. Mater. Interfaces*, 2019, **11**, 20873-20880.
8. H. Zhuang, P. Zhao and Y. Xu, *Inorg. Chem. Front*, 2020, **7**, 897.
9. H. Chen, A. Pei, J. Wan, D. Lin, R. Vilá, H. Wang, D. Mackanic, H.-G. Steinrück, W. Huang, Y. Li, A. Yang, J. Xie, Y. Wu, H. Wang and Y. Cui, *Joule*, 2020, **4**, 938-952.
10. H. Cheng, H. Jin, H. Liu, N. Cai, C. Gao, P. Zhang and M. Wang, *J. Electroanal. Chem.*, 2020, **878**, 114569.
11. X. Song, X. Zeng, J. Zou, F. Zhao and H. Wu, *J. Alloys Compd.*, 2021, **854**, 157122.
12. G. Luo, X. Hu, W. Liu, G. Lu, Q. Zhao, J. Wen, J. Liang, G. Huang, B. Jiang, C. Xu and F. Pan, *J. Energy Chem.*, 2021, **58**, 285-291.
13. H. Chen, Y. Yang, D.T. Boyle, Y.K. Jeong, R. Xu, L.S. de Vasconcelos, Z. Huang, H. Wang, H. Wang, W. Huang, H. Li, J. Wang, H. Gu, R. Matsumoto, K. Motohashi, Y. Nakayama, K. Zhao and Y. Cui, *Nat. Energy*, 2021, **6**, 790-798.
14. Y. Fang, S.L. Zhang, Z.-P. Wu, D. Luan and X.W. Lou, *Sci. Adv.*, 2021, **7**, eabg3626.
15. T. Yang, L. Li, T. Zhao, Y. Ye, Z. Ye, S. Xu, F. Wu and R. Chen, *Adv. Energy Mater.*, 2021, **11**, 2102454.